Article

Cyanide Storage on Ferroan Brucite (Mg$_x$Fe$_{1-x}$(OH)$_2$): Implications for Prebiotic Chemistry

Ellie K. Hara [1,2,*] **and Alexis S. Templeton** [1]

1 Department of Geological Sciences, University of Colorado Boulder, Boulder, CO 80309, USA; alexis.templeton@colorado.edu
2 Rensselaer Polytechnic Institute, Rensselaer Astrobiology Research and Education (RARE) Center, Troy, NY 12180, USA
* Correspondence: ellie.hara@colorado.edu

Abstract: Cyanide is a crucial reagent for the synthesis of biomolecules in prebiotic chemistry. However, effective organic synthesis requires cyanide to be concentrated. One proposed mechanism for cyanide storage and concentration on Early Earth involves the formation of aqueous ferrocyanide complexes. In basic pH conditions, cyanide will spontaneously form ferrocyanide complexes in the presence of aqueous Fe(II). While ferrocyanide aqueous complex formation is well defined, the potential for Fe(II)-bearing minerals to react with cyanide to form ferrocyanide complexes or store cyanide on the mineral surface has yet to be explored under prebiotically relevant conditions. In this study, we demonstrate that when cyanide interacts with ferroan brucite (Mg$_x$Fe$_{1-x}$(OH)$_2$), cyanide will both form aqueous and mineral-surface-adsorbed ferrocyanide implying that there are two reservoirs that cyanide will partition into. In addition, we found that cyanide decreased the amount of hydrogen gas produced by the oxidation of ferroan brucite, indicating that cyanide alters the mineral's redox reactivity. The cyanide adsorbed on brucite can be released by a decrease in pH, which leads to the dissolution of ferroan brucite, thus releasing the adsorbed cyanide. Our findings suggest that iron-bearing minerals may represent an overlooked storage reservoir of cyanide on Hadean Earth, potentially playing a significant role in cyanide availability for prebiotic chemistry.

**Keywords:** ferroan brucite; cyanide; ferrocyanide; prebiotic chemistry; adsorption

1. Introduction

Cyanide is a strong nucleophile and a key reactant for many prebiotically relevant reactions for the synthesis of molecules required for life as we know it. These include Strecker synthesis for amino acids, Oro's synthesis for nucleobases, and Eschenmoser synthesis for ribose-like sugars [1–3]. Modeling studies of prebiotic reaction networks have shown that the reaction of cyanide with copper, phosphorus, and hydrogen sulfide can synthesize the precursors of RNA, proteins, and lipids [4,5]. There were likely several sources of cyanide in the Hadean which include (i) cyanide formed in the interstellar medium delivered to Earth [6–8], (ii) formation of cyanide on Earth by electric discharge [9–11], and (iii) post-impact UV photochemistry [12–15], as well as (iv) the possibility of cyanide formed in submarine hydrothermal systems [16,17].

The simple presence of hydrogen cyanide (HCN) is not enough to drive prebiotic chemistry; it must be present at high enough concentrations. Experimental work on prebiotic reactions with HCN has used concentrations ranging from 125 μM HCN for making sugar precursors with the cyanocuprate redox cycle to 10 mM HCN for polymerization to 1M HCN

in the prebiotic network that forms RNA, protein, and lipid precursors [4,18–20]. At low HCN concentrations, we must also contend with the decay of HCN to formamide [21]. Thus, mechanisms for cyanide to be concentrated and stored are beneficial for prebiotic chemistry.

The formation of ferrocyanide has been proposed as a potential concentration mechanism for aqueous cyanide [22]. Cyanide, when in the presence of ferrous iron ions, spontaneously forms ferrocyanide $[Fe(CN)_6]^{4-}$ complexes [23]:

$$Fe^{2+} + 6CN^- \rightleftharpoons [Fe(CN)_6]^{4-}, K_{eq} = 2.5 \times 10^{35} \text{ at } 25\ ^\circ C \tag{1}$$
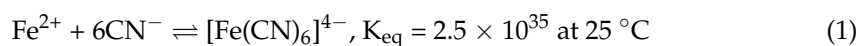
Because of the favorability of ferrocyanide complex formation under Earth surface conditions and the likely ferruginous ocean, ferrocyanide was likely abundant [24]. In this scenario, the majority of cyanide that dissolves in from the atmosphere would immediately be complexed into ferrocyanide. This implies that the ocean may have been a significant reservoir of ferrocyanide. One major inhibitor of ferrocyanide formation is the competition between ferrous iron and formaldehyde in reactions with cyanide. When formaldehyde is in excess of hydrogen cyanide, ferrocyanide will not form except in alkaline pH above 9 [25]. Formaldehyde forms spontaneously with UV light from water and CO_2 [26]. In neutral and acidic solutions, the reaction proceeds unless cyanide is physically separated from formaldehyde [22].

The influence of iron-bearing rocks and minerals on ferrocyanide formation has not been thoroughly investigated. During the Hadean, the crust was primarily mafic and ultramafic, and the hydration and oxidation of these rocks (aka "serpentinization") were thought to be widespread [27]. Mafic and ultramafic rocks contain a wide variety of iron-bearing minerals (e.g., olivine, pyroxene, magnetite, and brucite) that can dissolve and provide aqueous Fe(II) for ferrocyanide formation. The buffered water chemistry within serpentinites is alkaline and contains Fe(II) at micromolar to millimolar concentrations. The high pH is favorable for both ferrocyanide formation and stability, and thus ferrocyanide formation may be expected as water/rock reactions proceed [23,28].

Patel et al. (2015) hypothesized that ferrocyanide could be further accumulated as ferrocyanide salts that form from wet–dry cycles in closed basin lakes [4]. Toner and Catling (2019) have expanded on this and shown through modeling that sodium ferrocyanide salts could have accumulated in closed-basin lakes across a wide variety of conditions [29]. However, exposure to UV light leads to the photodecomposition of ferrocyanide [30,31]. Because of the greater flux of near-UV radiation during the Hadean, it is possible that any ferrocyanide on the Earth's surface would undergo this photodecomposition [32]. Thus, it is possible that due to the UV radiation exposure in a closed-basin lake system, ferrocyanide will not be able to accumulate. In contrast, subsurface serpentinites are shielded from photochemistry, and through Fe(II) complexation as well as Fe(II) mineral adsorption, may be able to store a significant amount of iron–cyanide complexes. Thus, we propose that subsurface-serpentinizing environments would be an ideal locale for cyanide concentration and storage.

We focus specifically on the interaction between cyanide and ferran brucite $(Mg_xFe_{1-x}(OH)_2)$, a mineral found in partially serpentinized rocks commonly associated with olivine and serpentine veins [33,34]. Ferroan brucite is formed under low silica conditions by an incomplete conversion of olivine to serpentine. Brucite is a significant ferrous iron reservoir, with the Mg/Fe molar ratio ranging from 0.95 to 0.65 [34–36]. Thermodynamic modeling has shown that ferrous iron preferentially partitions into brucite at temperatures below 200 °C [37]. This work assesses the feasibility for ferran brucite to act as a cyanide reservoir on Early Earth by measuring ferrocyanide complex formation and the impact of cyanide complex formation on hydrogen gas generation by the reaction of $(Mg_xFe_{1-x})(OH)_2$ in anoxic water.

2. Materials and Methods

Mg$_{66}$Fe$_{34}$(OH)$_2$ brucite was prepared in single batch in a Coy Chamber with an N$_2$/H$_2$ atmosphere by the slow addition of 14 mM or 140 mM NaOH to a 12 mM or 120 mM 0.66 Mg(II)/0.34 Fe(II) metal solution in a 1:1 ratio. 0.5 M NaOH was then used to adjust to the pH listed in Table 1 [38–40]. Brucite was allowed to equilibrate in the Coy Chamber for 4 h before usage. Then, 39 mL of the 60 mM prepared brucite solution was added to 60 mL serum vials and sealed with a blue butyl stopper. Cyanide from a stock solution and pH 10 water were added to attain the final concentrations of 10 mM, 5 mM, or 0 mM to obtain a total volume of 40 mL for each sample. Samples were flushed with N$_2$ gas to replace the headspace with an anaerobic atmosphere and then reacted in a 70 °C oven. To prevent any UV driven reactions, all serum vials were wrapped in foil. All glassware was washed with Citranox, soaked in an acid bath, and then rinsed with ultrapure water before use. We do note a significant decrease in pH across all experiments that we attribute to the continued hydrolysis of the 0.66 Mg(II)/0.34 Fe(II) metal mix; thus, we now recommend that precipitated ferroan brucite be left to equilibrate for two days and be washed with pH-adjusted water to remove excess salts before usage.

Table 1. The initial and final pH measurements for the three cyanide addition experiments. Ferrocyanide was detected in the 6 mM brucite experiments with 10 mM and 5 mM cyanide, with no ferrocyanide detected in the 0 mM cyanide control. Because cyanide is the limiting reagent in all experimental conditions tested, the theoretical maximum ferrocyanide was calculated by assuming all of the cyanide added would be complexed to form ferrocyanide.

[Brucite] (mM)	[CN$^-$] (mM)	Initial pH	Final pH	Measured [Fe(CN)$_6$]$^{4-}$ (mM)	Theoretical Maximum [Fe(CN)$_6$]$^{4-}$ (mM)
6 mM	10	10.09	8.69 ± 0.05	1.06 ± 0.10	1.67
6 mM	5	10.09	7.95 ± 0.06	0.24 ± 0.05	0.83
6 mM	0	10.09	7.41 ± 0.10	0	0
6 mM	10	11.26	10.12 ± 0.02	0.29 ± 0.01	1.67
6 mM	5	11.26	9.97 ± 1.29	0.19 ± 0.01	0.83
6 mM	0	11.26	9.64 ± 0.07	0	0
60 mM	10	10.00	8.40 ± 0.09	0	1.67
60 mM	5	10.00	8.36 ± 0.04	0	0.83
60 mM	0	10.00	8.29 ± 0.02	0	0

Initial headspace gas composition measurements were made on each sample prior to cyanide addition. Hydrogen gas concentrations from the samples' headspace were quantified on an SRI 8610 gas chromatograph (GC) using a 2 mm by 1 mm ED micropacked ShinCarbon ST column for separation with a thermal conductivity detector (TCD) and flame ionization detector (FID). An argon carrier gas was used at 12 psi. The temperature profile started at 50 °C for 3 min and then was increased to and held at 250 °C for 12 min. Calibrations were made using 1% standard gas mix (H$_2$/CO/CO$_2$/CH$_4$) and 100 ppm H$_2$ gas from Supleco Analytical. The detection limit, determined from the total number of moles in the lowest standard concentration measured for the calibration curve, was ~5 nmol H$_2$ gas.

After this initial headspace gas measurement, cyanide was added to samples until the targeted initial concentration was reached. Cyanide was added from pH 10 adjusted stock in the anaerobic chamber, and the total volume of each condition was kept constant with the addition of the NaOH solution. Samples were stored and reacted in a 70 °C oven.

Ferrocyanide concentrations were measured on a GENESYS 50 UV-VIS spectrophotometer. Samples were filtered with a 0.2 μm sterile membrane filter to remove any mineral particulates, and samples were diluted if necessary to be within the 0.01 mM and 0.1 mM

detection range. All spectra were processed in Origin Pro. Mineral characterization was completed on a Horiba LabRAM HR Evolution Spectrometer with a 100 mW 532 nm frequency-doubled Nd:YAG laser at 1%–10% power. Due to the age of the laser, the laser was functioning at approximately ~6 mW. The power was varied per sample for adequate signal/noise. Data were processed in LabSpec and plotted in R. Compound identification was carried out by comparing spectra collected from prepared standards. Mineral slurry from the experiments were first centrifuged to discard the aqueous fraction. The mineral fraction was dried anaerobically in the Coy Chamber to prepare for Raman spectroscopy analysis.

3. Results

The goal of these experiments was to test how cyanide would change in speciation when interacting with ferroan brucite. We hypothesized that cyanide would strongly bind with the Fe(II) in the ferroan brucite structure and liberate it to form aqueous ferrocyanide complexes. Thus, our first measurement was to quantify the amount of aqueous ferrocyanide detected in a solution and compare it to the theoretical maximum value of ferrocyanide, given the total amount of Fe(II) in the system. In each condition, there was excess Fe(II) compared to $[CN^-]$. We measured both pH and aqueous ferrocyanide concentrations in each sample reported in Table 1. Each condition had three replicates which were averaged, with the standard deviation reported. The initial pH of each experiment was pH 10 or 11.26, and a decrease in pH, ranging from 1.14 to 2.68 pH units, was measured at the end of the experiments.

In both 6 mM brucite experiments (10 mM $[CN^-]$ and 5 mM $[CN^-]$ addition), aqueous ferrocyanide was detected and quantified with UV-VIS measurements. Ferrocyanide was detected in all the 10 mM and 5 mM CN replicates, and no ferrocyanide was detected in the 0 mM $[CN^-]$ control. A plot of pH versus aqueous ferrocyanide concentration is shown in Figure 1, and measured concentrations of ferrocyanide are listed in Table 1. Compared to the theoretical maximum, there is less ferrocyanide measured in the solution than would be anticipated if all the cyanide formed a ferrocyanide complex and was released by the mineral into the aqueous phase. In contrast to the 6 mM brucite experiments, no ferrocyanide was detected in 60 mM brucite experiments conducted at pH 10.00. To test if there was $[CN^-]$ remaining in solution, we added excess $Fe(II)_{(aq)}$ to an aliquot of each sample to look for ferrocyanide complex formation, but ferrocyanide was still not detected in the aqueous phase. Both results indicate that there is another sink for $[CN^-]$.

Headspace hydrogen gas was measured for all experiments, but only the 60 mM brucite experiments reacted with 0 to 10 mM CN^- had data that were above detection limit. For the 60 mM Brucite experiments, hydrogen gas was measured pre-cyanide addition and then post-cyanide addition after 74 days of reaction in a 70 °C oven. These data, shown in Figure 2, shows that the addition of cyanide leads to less hydrogen gas production per mmol Fe in the brucite.

Raman spectra of dried mineral powders from the 60 mM brucite reacted with cyanide experiments are compared against reference spectra of ferroan brucite dried down with ferrocyanide. For additional comparison, a solid potassium ferricyanide standard was also measured (Figure 3). Multiple spectra were collected per sample, and a representative spectrum is plotted in Figure 3. We found that the cyanide was not homogenously distributed on the mineral surface, and so we had variable signal to noise for each spot analyzed, with some locations yielding no discernable nitrile peak.
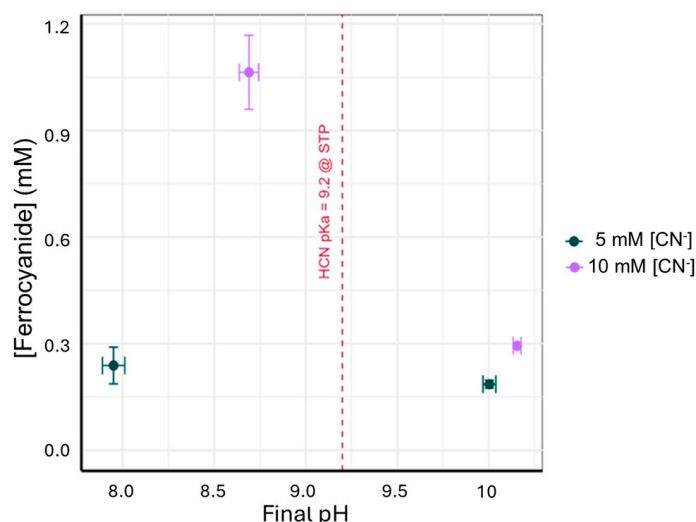
Figure 1. Average ferrocyanide concentration produced in experiments where 10 mM and 5 mM of CN was reacted with 6 mM brucite. The highest ferrocyanide concentration (1.06 ± 0.10 mM) occurred in the 6 mM brucite and 10 mM cyanide experiment, with an initial pH of 10.09 and final pH of 8.69.
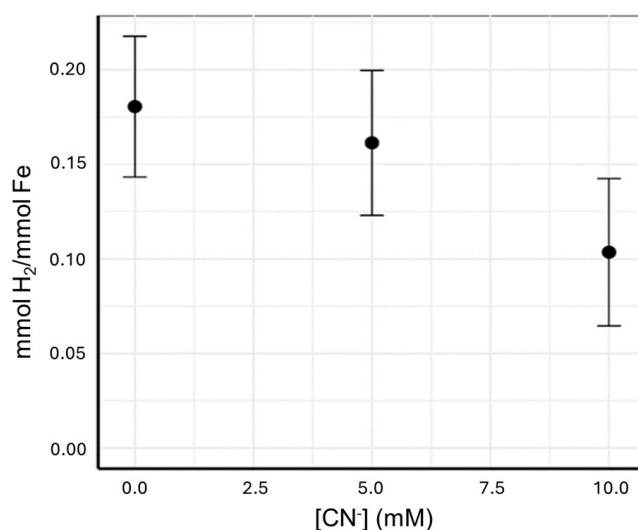

Figure 2. The amount of hydrogen gas produced per mmol of Fe available in brucite as a function of the amount of cyanide added to the system. Each point represents the average hydrogen gas production for the combined replicates, and the error bars represent one standard deviation.

The ferrocyanide/Fe brucite standard had peaks at 2066 cm^{-1}/2098 cm^{-1}, which are in good agreement with the reported ferrocyanide$_{(aq)}$ Raman peaks at 2058 cm^{-1}/2095 cm^{-1} [41]. When comparing our 10 mM CN$^-$ and 5 mM CN$^-$ added to ferroan brucite experiments, we measure peaks at 2081 cm^{-1}/2119 cm^{-1}, which, when compared to the reported aqueous standard, is a linear blue shift of 23 cm^{-1}/24 cm^{-1} and does not correlate with the potassium ferricyanide peaks. This blue shift in the characteristic ferrocyanide peaks is a reported result of ferrocyanide adsorption onto a surface [41–45]. Therefore, we conclude that when cyanide is added to ferroan brucite, we form adsorbed ferrocyanide complexes on the mineral surface.
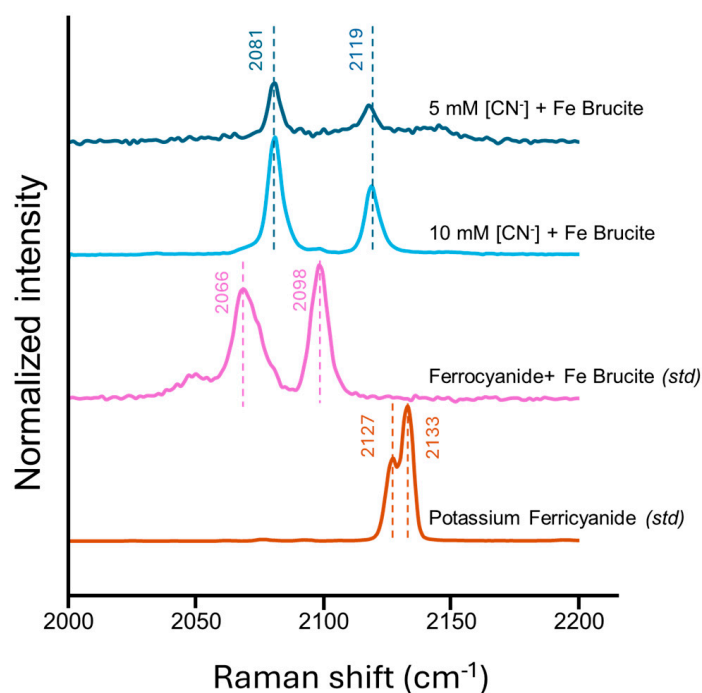
Figure 3. The Raman spectra of filtered and anaerobically dried mineral powders. The ferrocyanide + Fe Brucite standard was obtained by mixing the ferroan brucite slurry with aqueous standard potassium ferrocyanide and drying the mineral powder the same way that the experimental samples were dried. The top two spectra were from dried down samples of 60 mM ferroan brucite reacted with 5 and 10 mM cyanide. The bottom spectrum is of a solid potassium ferricyanide standard to show the contrast to ferrocyanide complexes. All spectra are normalized within the 2000–2200 cm^{-1} range.

4. Discussion

The goal of these experiments was to determine if the addition of cyanide to a dispersion containing ferroan brucite would lead to ferrocyanide complex formation, since only scenarios that consider aqueous complexation between cyanide and Fe(II)$_{(aq)}$ have been previously considered. We hypothesized that cyanide, through ligand-enhanced dissolution, could liberate mineral Fe(II)$_{(m)}$ (denoted with the subscript m) by forming a ferrocyanide complex that is then liberated from the mineral structure, leading to the formation of [Fe(CN)$_6$]$^{4-}$$_{(aq)}$. This process would liberate Fe(II)$_{(m)}$ to Fe(II)$_{(aq)}$ in the form of ferrocyanide complexes. The ligand-enhanced dissolution of magnesium from ultramafic rocks in alkaline conditions has been demonstrated with catechol, citrate, EDTA, and tiron [46]. Ligand-enhanced dissolution for brucite has been speculated in the literature previously, though not specifically with cyanide [47,48].

In the 6 mM brucite experiments, some aqueous ferrocyanide was detected. However, the yield for ferrocyanide was much lower than anticipated, with the highest yield occurring in experiments with an initial 10 mM of [CN$^-$] that reached a final pH of 8.69.

Because all experimental conditions had excess moles of Fe(II) compared to [CN$^-$] and the complexation is so strong, as shown in Equation (1), if ligand-enhanced brucite dissolution was occurring, all the cyanide should be accounted for in aqueous ferrocyanide. While some aqueous ferrocyanide was detected in the 6 mM brucite experiments, the yield for ferrocyanide was much lower than anticipated, with the highest yield occurring in experiments with an initial 10 mM of [CN$^-$] that reached a final pH of 8.69. We also observed a significant decrease in pH across all experiments. This implies that (1) there is another factor that controls aqueous ferrocyanide formation and (2) cyanide does not lead to ligand-enhanced dissolution.

To that first point, we propose that pH is the major factor controlling aqueous ferrocyanide formation. Higher pH is favorable for both aqueous cyanide availability (pKa 9.2) and ferrocyanide complex formation and stability. For experiments near pH 9, there exists a balance of $[CN^-]$ available from HCN deprotonation and $Fe(II)_{(aq)}$ available due to brucite solubility. Under this condition, more aqueous cyanide and iron are available to form ferrocyanide, and the ferrocyanide forms a stable complex. If the pH is too low, $[CN^-]$ will not be available in the aqueous phase for ferrocyanide formation. On the other hand, Fe(II) availability is favored by acidic pH conditions, whereas ferroan brucite is insoluble at high pH [47].

A predominance diagram for aqueous cyanide speciation as a function of pH illustrates the pH dependence (Figure 4) [49]. This diagram shows the pH and HCN concentrations where HCN, CN^-, and ferrocyanide are the dominant species at standard temperature and pressure. Fe(II) activity was set to 0.02 M to represent the total Fe(II) portion of the 60 mM ferroan brucite experiment. From this, it is apparent that ferrocyanide formation is favored under alkaline conditions and high HCN. In these experiments, increased cyanide concentrations led to an increase in measured aqueous ferrocyanide which aligns with the predictions from the stability diagram. The clearest difference in the amount of aqueous ferrocyanide formed comes from comparing the ferrocyanide concentration from 10 mM $[CN^-]$ experiments where the final pH was 8.69 and 10.16 with a final ferrocyanide concentration of 1.06 mM and 0.29 mM, respectively. At pH 10.16, there should be more $[CN^-]$ available. However, there is far less ferrocyanide formed likely due to the lack of ferrous iron available in the solution. In contrast, the experiment at pH 8.69 would have had $[CN^-]$ available, but with more ferrous iron available, more ferrocyanide formed. This would imply that ferrous iron would enhance the drawdown of HCN from the atmosphere by forming the ferrocyanide complexes. Therefore, we propose that pH is the predominant control of the ferrocyanide concentration by nature of controlling the amount of ferrous iron available from ferroan brucite.
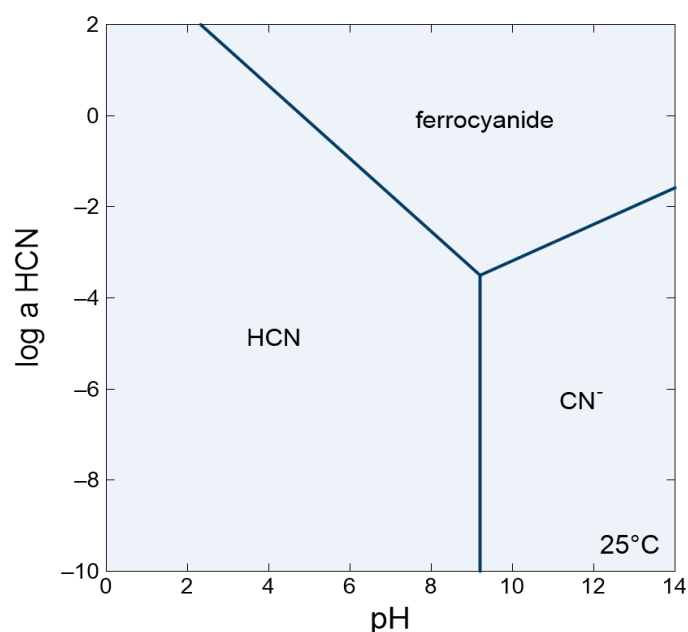

Figure 4. Predominance diagram made using Geochemist's Workbench® depicting the pH dependence for cyanide speciation and ferrocyanide formation. No surface interactions were included. The following parameters were used: activity of Fe(II) = 0.02, activity of H_2O = 1, temperature = 25 °C, pressure = 1 atm across a range of HCN log activity from −10 to 2.

While some aqueous ferrocyanide was detected in the 6 mM brucite experiments, no aqueous ferrocyanide was detected in the 60 mM brucite experiments. When additional $Fe(II)_{(aq)}$ was added, the experiments did not yield any detectable ferrocyanide, indicating that there was no $[CN^-]$ in the solution. This indicates that the mineral must be acting as a sink for $[CN^-]$. We propose that cyanide binds with structural $Fe(II)_{(m)}$ in the ferran brucite to form a surface-adsorbed ferrocyanide complex, and this complex does not release from the mineral surface. In ligand-enhanced mineral dissolution, there are two key steps (1) the adsorption of the ligand to an appropriate surface site and (2) detachment of the metal–ligand complex from the mineral surface. The latter is the rate limiting step and is dependent on the concentration of the ligand and solubility of the metal complex. The importance of complex solubility can be illustrated by comparing the dicyanoaurate complex to the ferricyanide complex. Cyanide leaching has been extensively used for gold recovery in the mining sector. The gold is selectively dissolved through the formation of a highly soluble dicyanoaurate complex. This soluble cyanide complex formation is also used for the extraction and recovery of silver and copper ores [50]. In contrast, when cyanide is added to pyrite at pH 10, ferricyanide complexes are formed on the surface, but these complexes are not soluble enough to detach from the mineral surface and enter the aqueous phase even when the surface is rinsed with additional DI water [51]. Therefore, cyanide does not lead to enhanced pyrite dissolution and instead is stored on the pyrite surface. Though both the dicyanoaurate and ferricyanide complex are cyanide–metal complexes, the difference in solubility leads to a difference in mineral dissolution properties. Similar to what is observed with pyrite, we propose that the ferrocyanide complex measured on the 60 mM ferran brucite experiment's mineral surface is not soluble enough to detach from the mineral surface and forms a bridge with the mineral surface as evidenced by the blue shift in the Raman bands.

When the ferran brucite/cyanide ratio is lowered, as we had in the 6 mM brucite experiments, some aqueous ferrocyanide was detected, despite there being less iron available in the system overall. It is possible that in the case of the 60 mM brucite, there are sufficient surface sites for the uptake of all $[CN^-]$ as surface adsorbed ferrocyanide. With less brucite (i.e., 6 mM), there are fewer surface sites, and thus, $[CN^-]$ in excess of the adsorbed fraction will remain in the solution. Additional evidence that a surface complex was formed comes from our observation that, in the 60 mM ferran brucite experiments, the addition of cyanide led to the suppression of hydrogen gas production, with higher concentrations of cyanide, leading to more suppression. The hydrogen gas is produced from coupling the oxidation of the Fe(II) component of ferran brucite with the reduction of water [48]. We propose that the cyanide is binding with the $Fe(II)_{(m)}$ in the structure to form ferrocyanide. Once this $Fe(II)_{(m)}$ is bound as ferrocyanide, it can no longer react with water to oxidize to Fe(III) and form hydrogen gas.

Altogether, the data imply that cyanide was able to complex with the mineral-bound iron in brucite but was not able to detach from the mineral surface into the aqueous system. Thus, cyanide is unable to enhance brucite dissolution, and the iron remains in the ferran brucite structure. Because cyanide does not lead to enhanced brucite dissolution, aqueous ferrocyanide is made entirely from Fe(II) that had been dissolved from ferrous brucite in response to the pH of the system. Thus, in the 6 mM ferran brucite experiments, pH is the driver of aqueous ferrocyanide complex formation by dictating the availability of ferrous iron. However, in the 60 mM brucite experiments, no aqueous ferrocyanide was formed, and there was no remaining aqueous cyanide. Instead, ferrocyanide was found to be adsorbed onto the mineral surface.

Implications for Prebiotic Chemistry

This work has demonstrated that when cyanide is added to a high-surface-area ferroan brucite, cyanide will be stored as mineral-surface-adsorbed ferrocyanide, and depending on the pH, some aqueous ferrocyanide can also form. Cyanide is an important reagent in prebiotic chemistry and, therefore, identifying systems that can store and concentrate cyanide of great interest. The mineral-surface-adsorbed ferrocyanide may serve as a concentration mechanism for ferrocyanide. In addition, serpentinizing systems have long been of interest to prebiotic chemistry with many published works detailing potential reaction mechanisms that capitalize on the naturally occurring chemical, temperature, and pH disequilibria found in these systems to start life on Earth [27,52–54]. What has not been explored is the role that cyanide plays in serpentinizing systems. The 60 mM ferroan brucite experiments demonstrated that it is possible to store at a minimum ~0.17 CN/ferroan brucite (mM/mM). Using the data from the 6 mM experiments, if we assume that all cyanide not accounted for in the measured aqueous ferrocyanide is associated with the mineral, then we have storage potentials listed in Table 2. This assumes that there are no other sinks for cyanide in the system. Additional study is needed to fully characterize the maximal cyanide storage by ferroan brucite under varying environmental conditions.

Table 2. The amount of cyanide that was measured in aqueous ferrocyanide was subtracted from the total amount of cyanide added to each experiment to obtain an approximation of how much cyanide was stored on the ferroan brucite surface. This concentration was divided by the amount of ferroan brucite to determine a CN/brucite ratio. This estimate assumes that there are no other sinks for cyanide.

[Brucite] (mM)	Final pH	[CN^-] (mM)	CN/Brucite (mM/mM)
6 mM	8.69 ± 0.05	10	3.64
6 mM	7.95 ± 0.06	5	3.56
6 mM	10.12 ± 0.02	10	8.26
6 mM	9.97 ± 1.29	5	3.86

Ferroan brucite, due to its sensitivity to pH, may also provide a useful surface to release the cyanide so that it can be used as a reactant in downstream chemistry. Brucite will dissolve rapidly at circumneutral pH, and so a decrease in environmental pH would lead to ferroan brucite dissolution [47]. This dissolution would release a large flux of the cyanide that was stored on the ferroan brucite surface, likely in the form of ferrocyanide. One geological example of this comes from the Lost City hydrothermal field where the vent chimneys are first composed of brucite and aragonite. As the vent ages, the brucite dissolves from prolonged exposure to seawater and the aragonite transforms to calcite [55].

While the cyanide locked into the ferrocyanide complex is unable to participate in chemical reactions, recent experimental work has shown that carbon monoxide can ligand exchange with the cyanide in ferrocyanide. This released cyanide into the aqueous system and forms a ferrocyanocarbonyl complex [56]. In addition, ferroan brucite may also host surface reactions that could occur only when the complex is bound to the mineral surface. Holm et al. (2006) has proposed that ferroan brucite could scavenge aqueous phosphate and borate and concentrate these reagents sufficiently to facilitate ribose formation through phosphorylation reactions [57].

In addition to ferroan brucite, there are other minerals that can serve as cyanide reservoirs. For example, pyrite (FeS_2) will store cyanide as ferricyanide [51]. Ferrocyanide was found to adsorb onto kaolinite, magnetite, and bentonite surfaces in prebiotically relevant conditions, where the mechanism of the interaction was also dependent on the pH

and the mineral structure. For bentonite and magnetite, ferrocyanide was also found to bind with Fe(III) present in the mineral structure and form Prussian blue analogues [58]. These studies, combined with our results, indicate that iron-bearing minerals may be currently overlooked for their potential to store and concentrate cyanide as iron–cyanide complexes.

5. Conclusions

Our experiments demonstrate that adding cyanide to a slurry of ferroan brucite mineral particles leads to ferrocyanide complex formation associated with the mineral surfaces, leading to the storage of cyanide under conditions where brucite is stable. Depending on pH, some aqueous ferrocyanide complexes are also formed. The formation of these ferrocyanide complexes does not enhance mineral dissolution. Instead, the results highlight the importance of pH in controlling the amount of aqueous ferrocyanide formed, since higher pH favors cyanide availability while decreasing ferrous iron availability; thus, aqueous ferrocyanide formation is optimal at moderately alkaline pH (e.g., pH 8–9). We also observed that increased cyanide association with the mineral surface decreases hydrogen gas production. Because hydrogen gas is produced by coupling the oxidation of $Fe(II)_{(m)}$ of ferroan brucite with the reduction of water, we propose that cyanide binds with $Fe(II)_{(m)}$ to form adsorbed ferrocyanide, thereby inhibiting iron oxidation. Overall, the results suggest that ferroan brucite, and potentially other iron minerals found in serpentinizing environments, may be underestimated reservoirs for cyanide storage and concentration which may have been important feedstocks for driving prebiotic chemistry.

References

1. Müller, D.; Pitsch, S.; Kittaka, A.; Wagner, E.; Wintner, C.E.; Eschenmoser, A.; Ohlofjgewidmet, G. Chemie von A-Aminonitrilen. Aldomerisierung von Glycolaldehyd-Phosphat Zu Racemischen Hexose-2,4,6-Triphosphaten Und (in Gegenwart von Formaldehyd) Racemischen Pentose-2,4-Diphosphaten: Rac-Allose-2,4,6-Triphosphat Und Rac-Ribose-2,4-Diphosphat Sind Die Reaktionshauptprodukte. *Helv. Chim. Acta* **1990**, *73*, 1410–1468. [CrossRef]
2. Oró, J. Synthesis of Adenine from Ammonium Cyanide. *Biochem. Biophys. Res. Commun.* **1960**, *2*, 407–412. [CrossRef]
3. Strecker, A. Ueber Einen Neuen Aus Aldehyd—Ammoniak Und Blausäure Entstehenden Körper. *Justus Liebigs Ann. Der Chem.* **1854**, *91*, 349–351. [CrossRef]
4. Patel, B.H.; Percivalle, C.; Ritson, D.J.; Duffy, C.D.; Sutherland, J.D. Common Origins of RNA, Protein and Lipid Precursors in a Cyanosulfidic Protometabolism. *Nat. Chem* **2015**, *7*, 301–307. [CrossRef] [PubMed]
5. Ritson, D.J.; Battilocchio, C.; Ley, S.V.; Sutherland, J.D. Mimicking the Surface and Prebiotic Chemistry of Early Earth Using Flow Chemistry. *Nat. Commun.* **2018**, *9*, 1821. [CrossRef] [PubMed]
6. Ehrenfreund, P.; Charnley, S.B. Organic Molecules in the Interstellar Medium, Comets, and Meteorites: A Voyage from Dark Clouds to the Early Earth. *Annu. Rev. Astron. Astrophys.* **2000**, *38*, 427–483. [CrossRef]
7. Pizzarello, S. Catalytic Syntheses of Amino Acids and Their Significance for Nebular and Planetary Chemistry. *Meteorit. Planet. Sci.* **2012**, *47*, 1291–1296. [CrossRef]

8. Pizzarello, S.; Shock, E. The Organic Composition of Carbonaceous Meteorites: The Evolutionary Story Ahead of Biochemistry. *Cold Spring Harb. Perspect. Biol.* **2010**, *2*, a002105. [CrossRef] [PubMed]

9. Cleaves, H.J.; Chalmers, J.H.; Lazcano, A.; Miller, S.L.; Bada, J.L. A Reassessment of Prebiotic Organic Synthesis in Neutral Planetary Atmospheres. *Orig. Life Evol. Biosph.* **2008**, *38*, 105–115. [CrossRef]

10. Ferus, M.; Kubelík, P.; Knížek, A.; Pastorek, A.; Sutherland, J.; Civiš, S. High Energy Radical Chemistry Formation of HCN-Rich Atmospheres on Early Earth. *Sci. Rep.* **2017**, *7*, 6275. [CrossRef] [PubMed]

11. Stribling, R.; Miller, S.L. Energy Yields in the Prebiotic Synthesis of Hydrogen Cyanide and Formaldehyde. *Orig. Life Evol. Biosph.* **1986**, *16*, 279–280. [CrossRef]

12. Tian, F.; Toon, O.B.; Pavlov, A.A.; De Sterck, H. A Hydrogen-Rich Early Earth Atmosphere. *Science* **2005**, *308*, 1014–1017. [CrossRef] [PubMed]

13. Tian, F.; Kasting, J.F.; Zahnle, K. Revisiting HCN Formation in Earth's Early Atmosphere. *Earth Planet. Sci. Lett.* **2011**, *308*, 417–423. [CrossRef]

14. Zahnle, K.J. Photochemistry of Methane and the Formation of Hydrocyanic Acid (HCN) in the Earth's Early Atmosphere. *J. Geophys. Res. Atmos.* **1986**, *91*, 2819–2834. [CrossRef]

15. Zahnle, K.J.; Lupu, R.; Catling, D.C.; Wogan, N. Creation and Evolution of Impact-Generated Reduced Atmospheres of Early Earth. *Planet. Sci. J.* **2020**, *1*, 11. [CrossRef]

16. Shock, E.L. Chapter 5 Chemical Environments of Submarine Hydrothermal Systems. *Orig. Life Evol. Biosph.* **1992**, *22*, 67–107. [CrossRef] [PubMed]

17. Holm, N.G.; Neubeck, A. Reduction of Nitrogen Compounds in Oceanic Basement and Its Implications for HCN Formation and Abiotic Organic Synthesis. *Geochem. Trans.* **2009**, *10*, 9. [CrossRef]

18. Sanchez, R.A.; Ferbis, J.P.; Orgel, L.E. Studies in Prebiotic Synthesis: II. Synthesis of Purine Precursors and Amino Acids from Aqueous Hydrogen Cyanide. *J. Mol. Biol.* **1967**, *30*, 223–253. [CrossRef]

19. Todd, Z.R.; Fahrenbach, A.C.; Magnani, C.J.; Ranjan, S.; Björkbom, A.; Szostak, J.W.; Sasselov, D.D. Solvated-Electron Production Using Cyanocuprates Is Compatible with the UV-Environment on a Hadean–Archaean Earth. *Chem. Commun.* **2018**, *54*, 1121–1124. [CrossRef] [PubMed]

20. Ritson, D.; Sutherland, J.D. Prebiotic Synthesis of Simple Sugars by Photoredox Systems Chemistry. *Nat. Chem.* **2012**, *4*, 895–899. [CrossRef] [PubMed]

21. Miyakawa, S.; James Cleaves, H.; Miller, S.L. The Cold Origin of Life: A. Implications Based On The Hydrolytic Stabilities Of Hydrogen Cyanide And Formamide. *Orig. Life Evol. Biosph.* **2002**, *32*, 195–208. [CrossRef] [PubMed]

22. Keefe, A.D.; Miller, S.L. Was Ferrocyanide a Prebiotic Reagent? *Orig. Life Evol. Biosph.* **1996**, *26*, 111–129. [CrossRef] [PubMed]

23. Sharpe, A.G. *The Chemistry of Cyano Complexes of the Transition Metals*; Academic Press: Cambridge, MA, USA, 1976.

24. Orgel, L.E. Sedimentary Minerals under Reducing Conditions. In *The Origin of Life and Evolutionary Biochemistry*; Dose, K., Fox, S.W., Deborin, G.A., Pavlovskaya, T.E., Eds.; Springer: Boston, MA, USA, 1974. [CrossRef]

25. Schlesinger, G.; Miller, S.L. Equilibrium and Kinetics of Glyconitrile Formation in Aqueous Solution. *J. Am. Chem. Soc.* **1973**, *95*, 3729–3735. [CrossRef]

26. Pinto, J.P.; Gladstone, G.R.; Yung, Y.L. Photochemical Production of Formaldehyde in Earth's Primitive Atmosphere. *Science* **1980**, *210*, 183–185. [CrossRef] [PubMed]

27. Sleep, N.H.; Bird, D.K.; Pope, E.C. Serpentinite and the Dawn of Life. *Philos. Trans. R. Soc. B Biol. Sci.* **2011**, *366*, 2857–2869. [CrossRef] [PubMed]

28. Todd, Z.R.; Wogan, N.F.; Catling, D.C. Favorable Environments for the Formation of Ferrocyanide, a Potentially Critical Reagent for Origins of Life. *ACS Earth Space Chem.* **2024**, *8*, 221–229. [CrossRef] [PubMed]

29. Toner, J.D.; Catling, D.C. Alkaline Lake Settings for Concentrated Prebiotic Cyanide and the Origin of Life. *Geochim. Cosmochim. Acta* **2019**, *260*, 124–132. [CrossRef]

30. Ašperger, S.; Murati, I.; Pavlović, D. Kinetics and Mechanism of the Decomposition of Complex Cyanides of Iron(II) and Molybdenum(IV). *J. Chem. Soc.* **1960**, 730–736. [CrossRef]

31. Gáspár, V.; Beck, M.T. Kinetics of the Photoaquation of Hexacyanoferrate(II) Ion. *Polyhedron* **1983**, *2*, 387–391. [CrossRef]

32. Catling, D.C.; Kasting, J.F. *Atmospheric Evolution on Inhabited and Lifeless Worlds*; Cambridge University Press: Cambridge, UK, 2017.

33. Bach, W.; Paulick, H.; Garrido, C.J.; Ildefonse, B.; Meurer, W.P.; Humphris, S.E. Unraveling the Sequence of Serpentinization Reactions: Petrography, Mineral Chemistry, and Petrophysics of Serpentinites from MAR 15°N (ODP Leg 209, Site 1274). *Geophys. Res. Lett.* **2006**, *33*. [CrossRef]

34. Beard, J.S.; Frost, B.R.; Fryer, P.; McCaig, A.; Searle, R.; Ildefonse, B.; Zinin, P.; Sharma, S.K. Onset and Progression of Serpentinization and Magnetite Formation in Olivine-Rich Troctolite from IODP Hole U1309D. *J. Petrol.* **2009**, *50*, 387–403. [CrossRef]

35. Boschi, C.; Dini, A.; Baneschi, I.; Bedini, F.; Perchiazzi, N.; Cavallo, A. Brucite-Driven CO_2 Uptake in Serpentinized Dunites (Ligurian Ophiolites, Montecastelli, Tuscany). *Lithos* **2017**, *288–289*, 264–281. [CrossRef]

36. Miller, H.M.; Mayhew, L.E.; Ellison, E.T.; Kelemen, P.; Kubo, M.; Templeton, A.S. Low Temperature Hydrogen Production during Experimental Hydration of Partially-Serpentinized Dunite. *Geochim. Cosmochim. Acta* **2017**, *209*, 161–183. [CrossRef]

37. McCollom, T.M.; Bach, W. Thermodynamic Constraints on Hydrogen Generation during Serpentinization of Ultramafic Rocks. *Geochim. Cosmochim. Acta* **2009**, *73*, 856–875. [CrossRef]

38. Olowe, A.A.; Génin, J.M.R. The Mechanism of Oxidation of Ferrous Hydroxide in Sulphated Aqueous Media: Importance of the Initial Ratio of the Reactants. *Corros. Sci.* **1991**, *32*, 965–984. [CrossRef]

39. Gilbert, F.; Refait, P.; Lévêque, F.; Remazeilles, C.; Conforto, E. Synthesis of Goethite from Fe(OH)2 Precipitates: Influence of Fe(II) Concentration and Stirring Speed. *J. Phys. Chem. Solids* **2008**, *69*, 2124–2130. [CrossRef]

40. Chimiak, L.; Hara, E.; Sessions, A.; Templeton, A.S. Glycine Synthesis from Nitrate and Glyoxylate Mediated by Ferroan Brucite: An Integrated Pathway for Prebiotic Amine Synthesis. *Proc. Natl. Acad. Sci. USA* **2024**, *121*, e2408248121. [CrossRef] [PubMed]

41. Loo, B.H.; Lee, Y.G.; Liang, E.J.; Kiefer, W. Surface-Enhanced Raman Scattering from Ferrocyanide and Ferricyanide Ions Adsorbed on Silver and Copper Colloids. *Chem. Phys. Lett.* **1998**, *297*, 83–89. [CrossRef]

42. Kettle, S.F.A.; Diana, E.; Boccaleri, E.; Stanghellini, P.L. The Vibrational Spectra of the Cyanide Ligand Revisited. Bridging Cyanides. *Inorg. Chem.* **2007**, *46*, 2409–2416. [CrossRef] [PubMed]

43. Dunbar, K.R.; Heintz, R.A. Chemistry of Transition Metal Cyanide Compounds: Modern Perspectives. In *Progress in Inorganic Chemistry*; John Wiley & Sons, Ltd.: Hoboken, NJ, USA, 1996; pp. 283–391. [CrossRef]

44. Lowry, R.B. SERS and Fourier Transform SERS Studies of the Hexacyanoferrate(III)-Hexacyanoferrate(II) Couple on Gold Electrode Surfaces. *J. Raman Spectrosc.* **1991**, *22*, 805–809. [CrossRef]

45. Allen, C.S.; Van Duyne, R.P. Molecular Generality of Surface-Enhanced Raman Spectroscopy (SERS). A Detailed Investigation of the Hexacyanoruthenate Ion Adsorbed on Silver and Copper Electrodes. *J. Am. Chem. Soc.* **1981**, *103*, 7497–7501. [CrossRef]

46. Bobicki, E.R.; Liu, Q.; Xu, Z. Ligand-Promoted Dissolution of Serpentine in Ultramafic Nickel Ores. *Miner. Eng.* **2014**, *64*, 109–119. [CrossRef]

47. Pokrovsky, O.S.; Schott, J. Experimental Study of Brucite Dissolution and Precipitation in Aqueous Solutions: Surface Speciation and Chemical Affinity Control. *Geochim. Cosmochim. Acta* **2004**, *68*, 31–45. [CrossRef]

48. Templeton, A.S.; Ellison, E.T. Formation and Loss of Metastable Brucite: Does Fe(II)-Bearing Brucite Support Microbial Activity in Serpentinizing Ecosystems? *Philos. Trans. R. Soc. A* **2020**, *378*, 20180423. [CrossRef] [PubMed]

49. Bethke, C.M. *Geochemical and Biogeochemical Reaction Modeling*, 2nd ed.; Cambridge University Press: Cambridge, UK, 2007. [CrossRef]

50. Medina, D.; Anderson, C.G. A Review of the Cyanidation Treatment of Copper-Gold Ores and Concentrates. *Metals* **2020**, *10*, 897. [CrossRef]

51. Guo, B.; Peng, Y.; Parker, G. Electrochemical and Spectroscopic Studies of Pyrite–Cyanide Interactions in Relation to the Depression of Pyrite Flotation. *Miner. Eng.* **2016**, *92*, 78–85. [CrossRef]

52. Russell, M.J.; Hall, A.J. The Emergence of Life from Iron Monosulphide Bubbles at a Submarine Hydrothermal Redox and pH Front. *J. Geol. Soc.* **1997**, *154*, 377–402. [CrossRef]

53. Russell, M.J.; Hall, A.J.; Martin, W. Serpentinization as a Source of Energy at the Origin of Life. *Geobiology* **2010**, *8*, 355–371. [CrossRef]

54. Russell, M.J.; Nitschke, W. Methane: Fuel or Exhaust at the Emergence of Life? *Astrobiology* **2017**, *17*, 1053–1066. [CrossRef] [PubMed]

55. Ludwig, K.A.; Kelley, D.S.; Butterfield, D.A.; Nelson, B.K.; Früh-Green, G. Formation and Evolution of Carbonate Chimneys at the Lost City Hydrothermal Field. *Geochim. Cosmochim. Acta* **2006**, *70*, 3625–3645. [CrossRef]

56. Hara, E.K.; Templeton, A.S. Releasing Cyanide from Ferrocyanide through Carbon Monoxide Ligand Exchange in Alkaline Aqueous Environments. *ACS Earth Space Chem.* **2024**, *8*, 900–906. [CrossRef]

57. Holm, N.G.; Dumont, M.; Ivarsson, M.; Konn, C. Alkaline Fluid Circulation in Ultramafic Rocks and Formation of Nucleotide Constituents: A Hypothesis. *Geochem. Trans.* **2006**, *7*, 7. [CrossRef]

58. Samulewski, R.B.; Pintor, B.E.; Ivashita, F.F.; Paesano, A.; Zaia, D.A.M. Study of Ferrocyanide Adsorption onto Different Minerals as Prebiotic Chemistry Assays. *Astrobiology* **2021**, *21*, 1121–1136. [CrossRef] [PubMed]